ARTICLES

Ultrametricity and memory in a solvable model of self-organized criticality

Stefan Boettcher[1,2] and Maya Paczuski[1]
[1]*Department of Physics, Brookhaven National Laboratory, Upton, New York 11973*
[2]*Department of Physics and Astronomy, The University of Oklahoma, Norman, Oklahoma 73019-0225*
(Received 4 March 1996)

Slowly driven dissipative systems may evolve to a critical state where long periods of apparent equilibrium are punctuated by intermittent avalanches of activity. We present a self-organized critical model of punctuated equilibrium behavior in the context of biological evolution, and solve it in the limit that the number of independent traits for each species diverges. We derive an exact equation of motion for the avalanche dynamics from the microscopic rules. In the continuum limit, avalanches propagate via a diffusion equation with a nonlocal, history dependent potential representing memory. This nonlocal potential gives rise to a non-Gaussian (fat) tail for the subdiffusive spreading of activity. The probability for the activity to spread beyond a distance r in time s decays as $\sqrt{(24/\pi)}s^{-3/2}x^{1/3}\exp[-3/4x^{1/3}]$ for $x=r^4/s\gg 1$. The potential represents a hierarchy of time scales that is dynamically generated by the ultrametric structure of avalanches, which can be quantified in terms of ''backward'' avalanches. In addition, a number of other correlation functions characterizing the punctuated equilibrium dynamics are determined exactly. [S1063-651X(96)05108-2]

PACS number(s): 05.40.+j, 05.70.−a, 87.10.+e

I. INTRODUCTION

Many natural phenomena evolve intermittently rather than following a uniform, gradual path. In particular, the dynamics of systems out of equilibrium may follow a steplike pattern with long, dormant plateaus interrupted by sudden bursts, or avalanches, where the accumulated stress is released. Avalanche dynamics violates the picture of gradualism where large systems evolve continuously, for instance, to a local energy minimum. The bursts which separate subsequent metastable states may eventually span all scales up to the system size [1] thus providing a general mechanism for long-range spatiotemporal correlations. The appearance of fractals, $1/f$ noise, Levy flights, etc., have been unified by relating these phenomena, in a broad class of nonequilibrium models, to an underlying avalanche structure [2].

Even though the theory of uniformitarianism, or gradualism, has historically dominated both geology and paleontology, prototypical examples of avalanche dynamics lie in these two domains [3]. For instance, the distribution of earthquake magnitudes follows a power law found by Gutenberg and Richter [4]. The scale-free variation from small events to large events indicates a common dynamical origin and eventually led to the suggestion that earthquakes are an example of self-organized criticality [5]. Most of the time, the crust of the earth appears stable. These periods of apparent equilibrium are punctuated by earthquakes, which take place on a fractal fault structure [6] that stores information about the history of the system.

Actually, over twenty years ago, Gould and Eldredge proposed that biological evolution also takes place in terms of punctuations, where many species become extinct and new species emerge, interrupting periods of low activity [7]. In this context, punctuated equilibrium usually refers to the intermittent dynamics of single species, where morphological change is concentrated in short intervals in time interrupting long periods of stasis. These punctuations may be correlated to large extinction events in the global ecology, which may themselves be distributed according to a power law analogous to the Gutenburg-Richter law for earthquakes [3,8].

This view was promoted by Bak and Sneppen [9] who introduced a simple self-organized critical (SOC) model for coevolutionary avalanches of different species in an ecology. The model explicitly treats macroevolution as a many-body statistical problem where the fitness landscape in which each species evolves is affected by changes in other species in the ecology. The mutation of the ''least fit'' species in the system completely changes the fitness landscape of some other species and coevolution with punctuated equilibrium behavior is obtained. This occurs without fine tuning parameters and without the need for external shocks leading to cataclysms of mass extinction. The extinction events (avalanches) have a power law distribution of sizes, where most extinction is concentrated in the largest events. This fact provides some theoretical underpinning for catastrophism rather than uniformitarianism as the defining characterization of evolutionary history [10]. The model may capture some robust features of real evolution, such as punctuated equilibrium and catastrophism, in spite of its drastic simplifications.

In fact, Ito [11] has related the spatiotemporal pattern of earthquakes in California to the avalanche pattern found in the Bak-Sneppen evolution model. The data for the pattern of successive earthquakes over time may be fractal in space and time, so that each earthquake can be viewed as a single event within a much larger avalanche structure consisting of many earthquakes. If this picture is correct, earthquakes can be described as a ''fractal renewal process'' [2,12] with a power law distribution of times between subsequent earth-

quakes in a given region. The analogy can be made by replacing the least fit species with the weakest link in the earth's crust. Ito's observations of return times for earthquakes in California are consistent with general scaling relations valid for the Bak-Sneppen model, as well as other extremal SOC models [2] for invasion percolation [13], interface depinning [14], and flux creep [15].

Although the Bak-Sneppen model is an extremely simple model of SOC and a few exact results as well as many scaling relations are known for it [2], it has not (yet) been solved. A variety of similar evolution models have been subsequently introduced to incorporate more aspects of reality such as speciation and external shocks [16]. These models have been primarily studied numerically.

Recently, we have proposed a multitrait evolution model with M independent, internal degrees of freedom for each species [17]. This model is solvable in the limit $M\rightarrow\infty$; it includes the Bak-Sneppen model when $M=1$. We have previously reported some of the simplest results [17]. Here we present a more extensive analysis of the model. Note that the $M\rightarrow\infty$ limit is not mean-field theory [18] because it contains spatial correlations and punctuated equilibrium dynamics. In addition, we find rigorous results that might be too delicate to detect with numerical calculations alone, such as the non-Gaussian tail for the distribution of activity.

The multitrait evolution model incorporates the notion that the survivability of each species depends on a number of independent traits associated with the different tasks that it has to perform in order to survive [19]. Evolution proceeds via an extremal dynamics where the species in the global ecology with the lowest barrier to mutation, or the least fit, mutates. This event affects certain barriers to mutation or fitnesses of other species in the system which are related through, for instance, a food chain. As a consequence of the interaction between species, even species that possess well-adapted abilities, with high barriers, can be undermined in their existence by weak species with which they interact. This may lead to a chain reaction of coevolution. The pattern of change of individual species exhibits punctuated equilibrium behavior which comes from episodes of mass extinction events sweeping through the species. Punctuated equilibrium is described by a Devil's staircase, as shown in Fig. 1. The introduction of many internal traits for each species is consistent with paleontological observations indicating that evolution within a species is ''directed'' [19]; morphological change over time is concentrated in a few traits, while most others traits of the species are static.

Our main analytical results are as follows: For $M\rightarrow\infty$, we derive an exact equation of motion, given in Eq. (3.7), for the macroscopic observables in the SOC state from the microscopic dynamics. From this equation, which is our central result, one can extract separate equations for the temporal and spatial distribution of avalanche sizes, both of which are determined exactly in Eqs. (2.2), (2.3) and were previously derived by us in Ref. [17]. In the continuum limit, the subdiffusive dynamics is given by a ''Schrödinger'' equation with a nonlocal potential in time Eq. (3.8). This potential represents memory. The exact asymptotic solution Eq. (3.9) of the Schrödinger equation at large length and time scales has a non-Gaussian tail. This solution describes the nontrivial spatiotemporal pattern of activity in the self-organized

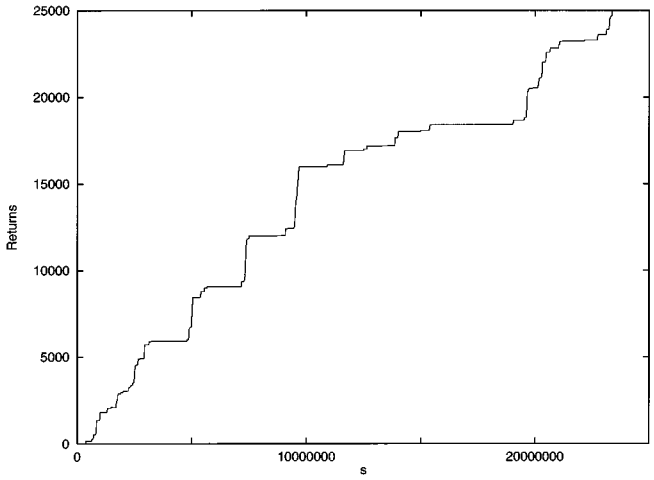

FIG. 1. Punctuated equilibrium behavior for the evolution of a single species in the one-dimensional $M=\infty$ model. The vertical axis is the total number of returns of the activity to some site as a function of time s. Note the presence of plateaus (periods of stasis) of all sizes. The distribution of plateau sizes scales as $s^{-7/4}$.

critical state. The anomalous diffusion arises from a long-term memory effect due to the ultrametric tree structure [20] of avalanches. This tree structure of activity is quantified by calculating the ultrametric distances between subsequent extremal (minimal) sites. The probability distribution for this distance is a power law at large times and asymptotically approaches the probability distribution of all backward avalanches. This latter quantity, which we will define in the text, is calculated exactly in Eq. (5.3). A number of other distribution functions are also determined. The critical exponents are $D=4$, $\tau=3/2$, $\tau_R=3$, $\gamma=1$, $\nu=\sigma=1/2$, $\tau_f^{all}=2$, $\tau_b^{all}=3/2$, and $\tau_{FIRST}=2-d/4$. The nonlocal time dependence of the dynamical equations and the ultrametric structure of avalanches suggest a possible relation between glassy dynamics and self-organized criticality [21].

In Sec. II, we introduce our model and show that it self-organizes to the critical state. It is demonstrated that avalanches in the critical state have an ultrametric tree structure. In Sec. III, we derive the equation of motion for the critical state for the $M\rightarrow\infty$ model and present our main analytical results for the anomalous diffusion. In Sec. IV, we show that the critical behavior is characterized by simple power laws with specific exponents that verify general scaling relations for nonequilibrium phenomena. In Sec. V we calculate the distributions for ''backward avalanches.'' Due to irreversibility these differ from the usual ''forward'' avalanche distributions. The backward avalanches can be related to the ultrametric distances between subsequent activity. Most details of our calculations have been deferred to the Appendices.

II. THE MULTITRAIT EVOLUTION MODEL

Our model is defined as follows: A species is represented by a single site on a d-dimensional lattice. The collection of traits for each species is represented by a set of M numbers in the unit interval. A larger number represents a better ability to perform that particular task, while smaller numbers pose less of a barrier against mutation. Therefore, we ''mu-

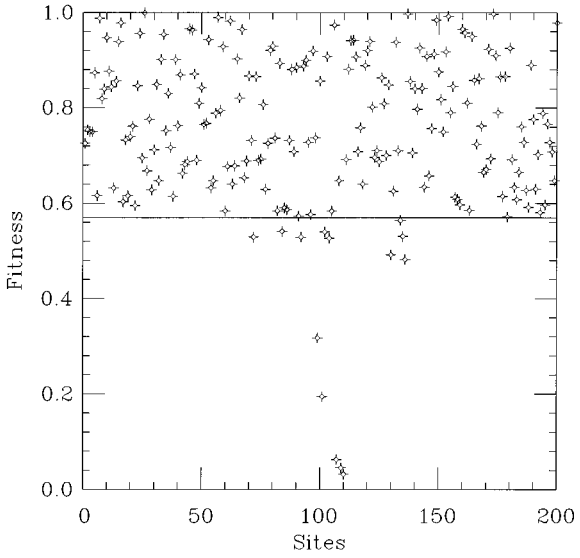

FIG. 2. Snapshot of the stationary state in a finite one-dimensional system for the $M=1$ (Bak-Sneppen) model. Except for the avalanche which consists of small fitness values in a localized region, almost all the fitness values in the system are above a self-organized threshold λ_c.

tate'' at every time step the smallest number in the entire system by replacing it by a new (possibly smaller) number that is randomly drawn from a flat distribution in the unit interval $\mathcal{P}$. Choosing the smallest random number mimics the Darwinian principle that the least fit species mutates [22].

The dynamical impact of this event on neighboring species is simulated by also replacing one of the M numbers on each neighboring site with a new random number drawn from $\mathcal{P}$. Which one of the M numbers is selected for such an update is determined at random, since we assume that a mutation in the traits of one species can lead to an adaptive change in any one of the traits of a dependent species. The interaction between the fitnesses of species leads to a chain reaction of coevolution.

A. Self-organization

The sequence of selective random updates at extremal (minimal) sites with nearest-neighbor interactions drives the system from any initial state to a self-organized critical state in which species exist in a state of punctuated equilibrium with bursts of evolutionary activity that are correlated over all spatial and temporal extents. In this state almost all species have reached fitnesses above a SOC threshold, enjoying long periods of quiescence, interrupted by intermittent activity when changes in neighboring species force a readjustment in their own barriers. A snapshot of the stationary state in a finite one-dimensional system is shown in Fig. 2.

The self-organization process for the finite M model is similar to that for the Bak-Sneppen model ($M=1$). It is described by a ''gap'' equation that relates the rate of approach towards the stationary attractor to the average avalanche size. This equation demonstrates that the stationary state of the system is a critical state for the avalanches, where the average avalanche size diverges. Following Ref. [2] we define the gap $G(s)$ to be the largest of the minimal random numbers selected up to time s, given an initial state at $s=0$ where all the random numbers are uniformly distributed in the unit interval. Therefore, $G(s=0)=O(1/ML^d)$. As evolution proceeds, the gap $G(s)$ increases monotonically in a stepwise fashion with intermediate plateaus that become longer and longer. These plateaus occur when subsequent minimal random numbers in the system are smaller than a minimum at some previous time. One can assign to each plateau an avalanche which starts and ends with consecutive changes in $G(s)$, and which consists of all the random numbers in the gap below $G(s)$. As the gap increases, the probability for the new random numbers to fall below the current gap increases also, and longer and longer avalanches typically occur.

Following Ref. [2] again, it can be shown from the law of large numbers that in the limit of large system sizes L, the growth of the gap versus time s obeys the gap equation

$$\frac{dG(s)}{ds}=\frac{1-G(s)}{ML^d\langle S\rangle_{G(s)}}. \tag{2.1}$$

As the gap increases, so does the average avalanche size $\langle S\rangle_{G(s)}$, which eventually diverges as $G(s)\to G_c$. In the limit $L\to\infty$, the density of sites with random numbers less than G_c vanishes, and the distribution of random numbers is uniform above G_c. The gap equation (2.1) contains the essential physics of SOC phenomena. When the average avalanche size diverges, $\langle S\rangle_{G(s)}\to\infty$, the system becomes critical. At the same time dG/ds approaches zero, which means that the system becomes stationary. For any finite M the process of self-organization is the same as for the $M=1$ model, and all of the results derived for that case apply. Since M just enters as a rescaling of the system size L in Eq. (2.1), it is plausible that the critical behavior for any finite M is in the same universality class as for $M=1$. We have shown [17] that the limit $M\to\infty$ is a different universality class.

B. Ultrametricity of avalanches

It is useful to consider the case where, at a certain time, the smallest random number in the system has the value λ. A λ avalanche by definition consists of all subsequent random numbers which are below λ. The λ avalanche that started at s ends at the first instant $s+s'$ when the smallest random number in the system is larger than λ. All of the random numbers that are below the threshold value λ at any one instant in time are called ''active'' because they make up the λ avalanche.

We now consider the sequence of minimal values $\lambda_{min}(s)$ comprising any λ avalanche. Each value $\lambda_{min}(s)$ has a parent barrier value $\lambda_{min}(s-s')$ preceding it within the λ avalanche. This parent is the barrier that introduced the particular random number into the system that became the minimum at time s. Obviously, the parent of the $\lambda_{min}(s)$ value also has its own parent. One can therefore place all of the barrier values within a given avalanche onto a tree, as shown in Fig. 3. The distance on the tree between any two active barrier values at a given time is determined by the most recent common ancestor of the two values. This distance is ultrametric [20]. In Sec. V we relate the probability

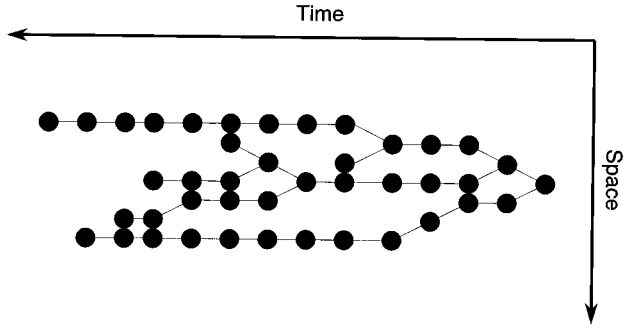

FIG. 3. Ultrametric tree structure. At any given time, indicated by the vertical axis, all of the active sites below threshold have an ancestry which forms a tree. The ultrametric distance between any pair is the distance back in time to the first common ancestor.

distribution of the ultrametric distances between subsequent minimal random numbers to the distribution of all backward avalanches, which is determined exactly.

C. The limit $M\to\infty$

For finite M, active barriers can be eliminated both by becoming the global minimum at some time, or by being chosen in the nearest-neighbor interaction when the global minimum occurs on a neighboring site. The case $M\to\infty$ of the model is special because the existing active barriers that any species possesses can only be changed if these barriers themselves become the global minimum, despite the nearest-neighbor interaction in the model. Since there are infinitely many barriers *on each site*, no existing active barrier is ever likely to be chosen for an update in a nearest-neighbor interaction. The nearest-neighbor interaction can only create new active barriers. This fact allows us to formulate a cascade mechanism which can be solved exactly.

In what follows we shall consider the stationary state behavior in the limit of infinite system size, and confine our presentation to the $d=1$ dimensional case of our model with $M\to\infty$. We point out later which critical exponents are dimension dependent and dimension independent, and we will discuss in more detail the results for higher dimensional lattices elsewhere [23]. To simplify the algebra further, we make a slight modification of the model without restricting the generality of the results: At each time step during the avalanche, the smallest active barrier is set to unity instead of being replaced by a new random number. Then, there is either no new active barrier created with probability $(1-\lambda)^2$, or one such barrier is created to the left or to the right of the minimum with probability $\lambda(1-\lambda)$ in either case, or two active barriers are created to the left and the right of the minimum with probability λ^2.

The spatial and temporal correlations in our model can be separated into two independent equations of motion for the width and duration of avalanches. For instance, the distribution of avalanches sizes s is given by (see Appendix A)

$$P_\lambda(s)=4^s\lambda^{s-1}(1-\lambda)^{s+1}A(s)$$

$$A(s)=\frac{\Gamma(s+\frac{1}{2})}{\Gamma(\frac{1}{2})\Gamma(s+2)}. \tag{2.2}$$

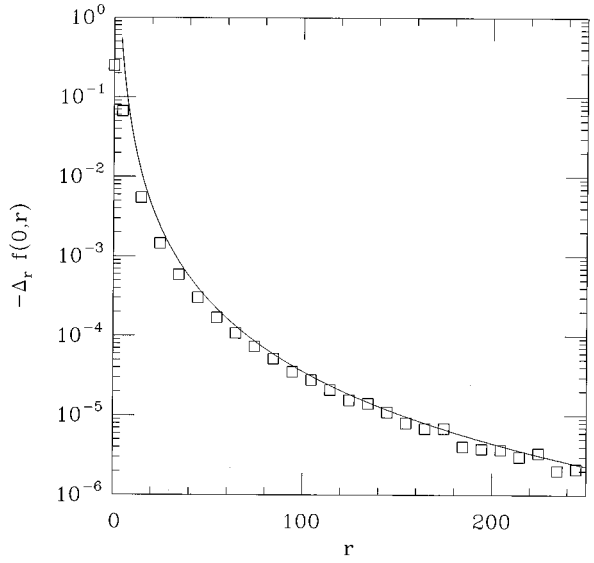

FIG. 4. Numerical verification of Eq. (2.4). We sampled the probability for an avalanche to start at the origin and to be contained by the smallest possible box of radius r for $r\leqslant 250$ with increments of $\Delta r=10$. Squares represent the measured values from a sample of 2×10^6 avalanches for this probability, corresponding to $-\partial_r f(0,r)\sim 35.48\ldots r^{-3}$ which is drawn as a solid line.

For $\lambda=\lambda_c=1/2$, $P_{\lambda_c}(s)\sim s^{-\tau}$ for large sizes with $\tau=3/2$. For $\lambda<\lambda_c$, the critical avalanches are subdivided into smaller avalanches and the distribution acquires a cutoff. The critical behavior is quite different than the $M=1$ model where the numerical result is $\tau\simeq 1.1$ in one dimension [2]. The model for $M=\infty$ clearly represents a different universality class than the original Bak-Sneppen model. Actually, the temporal behavior in this case is identical to the temporal behavior of the random-neighbor evolution model [18].

Unlike the random-neighbor model, though, the $M\to\infty$ model also exhibits spatial correlations, leading to punctuated equilibrium behavior. In Ref. [17] we found that the probability f_r of a λ_c avalanche to ever affect a particular site of distance r from its origin is exactly given by

$$f_r=\frac{12}{(r+3)(r+4)}, \tag{2.3}$$

implying that the probability for an avalanche to reach precisely to a site of distance r falls asymptotically as $r^{-\tau_R}$ with $\tau_R=3$. Noting that one particular site can not fully contain the spread of an avalanche, we have obtained an equation for the probability $f(0,r)$ of a λ_c avalanche to start at the origin and to ever leave a box of radius r around its origin. The leading asymptotic behavior of the solution for confined avalanches is given by

$$f(0,r)\sim\frac{1}{3}\left[\frac{\Gamma(\frac{1}{6})\Gamma(\frac{1}{2})}{\Gamma(\frac{2}{3})}\right]^2\frac{1}{r^2}\quad(r\to\infty), \tag{2.4}$$

confirming that $\tau_R=3$. The calculation leading to Eq. (2.4) is given in Appendix B. A comparison of numerical results for $f(0,r)$ with the asymptotic behavior, given in Fig. 4, show perfect agreement.

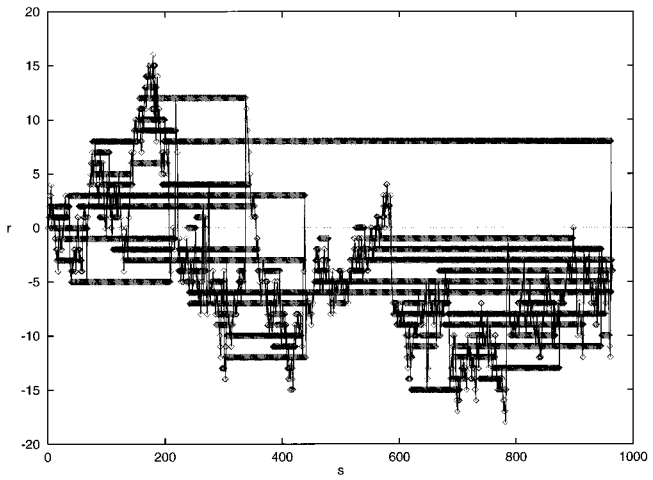

FIG. 5. Plot of a typical λ_c avalanche for $M=\infty$, starting at the origin at time $s=0$, and ending at time $s=976$. At each time step, every site with at least one active barrier is marked $\diamond$, and the sequence of minimal sites is connected with a line showing jumps of various sizes. Apparent also are the punctuated equilibria for each site which extend over many sizes. The propagator $G(r,s)$ of the activity is the probability to have a minimum at site r at time s, while $F(r,s)$ is the probability for an avalanche to end at s (here: $=976$) and to have reached a particular site r at any time during its evolution.

III. THE CASCADE EQUATION AND MAIN RESULTS

Ultimately, spatial and temporal correlations are interrelated through the microscopic rules for the propagation of activity in space and time. Ideally, one would like to determine the propagator $G(r,s)$ which is the probability that the minimum barrier value will be located at position r at time s given that it was at location 0 at time 0 for the infinite λ_c avalanche. We have not been able to analytically calculate this quantity directly. We have instead focused on a different quantity. Let $F_\lambda(r,s)$ be the probability for a λ avalanche to survive precisely s steps and to have affected a particular site of distance r from its origin. Conceptually, the quantity $F_{\lambda_c}(r,s)$ may roughly correspond to an envelope function of the propagator $G(r,s)$. This relation between F and G is explained in Fig. 5. Due to the lack of any scale in the model, it is plausible that the asymptotic behavior of G and F is identical, as comparison with numerical calculations suggests.

The direct analysis of this envelope function proves to be rewarding in many respects. We find a cascade equation which can be reduced to separate equations for spatial and temporal correlations. In the continuum limit, the avalanche dynamics is given in terms of a Schrödinger equation with a nonlocal potential in time. We solve this equation to find the leading asymptotic behavior of $F_{\lambda_c}(r,s)$. This calculation yields a non-Gaussian tail in the distribution with an avalanche dimension $D=4$, signaling subdiffusive behavior for the spread of activity.

First, we consider $P_\lambda(r,s)$, the probability that the λ avalanche dies precisely after s updates and does *not* affect a particular site r away from the origin of the avalanche. The quantities $P_\lambda(r,s)$ and $F_\lambda(r,s)$ are simply related

$$P_\lambda(r,s)=P_\lambda(r=\infty,s)-F_\lambda(r,s), \tag{3.1}$$

where $P_\lambda(r=\infty,s)=P_\lambda(s)$, as given in Eq. (2.2). Since we consider the avalanche to start with a single active barrier at $r=0$ and $s=0$, it is $P_\lambda(r=0,s)\equiv 0$ for all $s\geq 0$, and $P_\lambda(r,s=0)\equiv 0$ for all r because the avalanche has not died at $s=0$. The remaining properties of a λ avalanche can be deduced from the properties of avalanches that ensue after the first update. It will terminate with probability $(1-\lambda)^2$ after the first update when the update does not produce any new active barriers. Thus it is $P_\lambda(r,s=1)\equiv(1-\lambda)^2$. For avalanches surviving until $s\geq 2$ we find for $r\geq 1$

$$P_\lambda(r,s)=\lambda(1-\lambda)[P_\lambda(r-1,s-1)+P_\lambda(r+1,s-1)] + \lambda^2\sum_{s'=0}^{s-1} P_\lambda(r-1,s')P_\lambda(r+1,s-1-s') \tag{3.2}$$

in the following way: The first update may create exactly one new active barrier with probability $\lambda(1-\lambda)$ either to the left or to the right of the origin (i.e., one step towards or away from the chosen site of distance r). In this case, the properties of the original avalanche of duration s are related to the properties of an avalanche of duration $s-1$ with regard to a site of distance $r-1$ or $r+1$, respectively. Finally, the first update may create two new active barriers with probability λ^2 to the left and the right of the origin. Then, the properties of the original avalanche of duration s are related to the properties of all combinations of two avalanches of combined duration $s-1$. Both of these avalanches evolve in a *statistically independent* manner for $M=\infty$. Since only one of these avalanches can be updated at each time step, their combined duration has to add up to $s-1$ for this process to contribute to the avalanche of duration s. For any such combination, the probability to not affect the chosen site of distance r from the origin is given simply by the product of the probabilities for the two ensuing avalanches to not affect a chosen site of distance $r-1$ or $r+1$, respectively.

Before proceeding with the solution of Eq. (3.2), we review some limiting cases to obtain previously derived results [17]. Considering the limit $r=\infty$, for $s\geq 2$, Eq. (3.2) reduces to

$$P_\lambda(s)=2\lambda(1-\lambda)P_\lambda(s-1)+\lambda^2\sum_{s'=0}^{s-1} P_\lambda(s')P_\lambda(s-1-s'). \tag{3.3}$$

This is the cascade equation for the lifetime distribution of avalanches whose solution is Eq. (2.2) (see Appendix A). Near the critical point, $\Delta\lambda=\lambda_c-\lambda\to 0_+$, the lifetime distribution obeys a scaling form

$$P_\lambda(s)\sim s^{-\tau}G(s\Delta\lambda^{1/\sigma}) \quad (\tau=\tfrac{3}{2},\sigma=\tfrac{1}{2}). \tag{3.4}$$

Similarly, we can rederive Eq. (2.3) for the spatial correlations. Defining $N_\lambda(r)=\Sigma_s P_\lambda(r,s)$, Eq. (3.2) yields $N_\lambda(0)=0$, and for $r\geq 1$

$$N_\lambda(r)=(1-\lambda)^2+\lambda(1-\lambda)[N_\lambda(r-1)+N_\lambda(r+1)] + \lambda^2 N_\lambda(r-1)N_\lambda(r+1). \tag{3.5}$$

$N_\lambda(r)$ is the probability for an avalanche of any temporal extent not to reach a particular point of distance r before it dies. Equation (3.5) for $\lambda=\lambda_c=1/2$ is solved by $N_{\lambda_c}(r)=1-f_r$ with f_r given in Eq. (2.3). Close to the critical point this quantity also obeys a scaling form

$$1-N_\lambda(r)\sim\frac{1}{r^{\tau_R-1}}H(r\Delta\lambda^\nu)\quad(\tau_R=3,\nu=\tfrac{1}{2}).\tag{3.6}$$

The equation governing the envelope function $F_\lambda(r,s)$ is obtained by inserting Eq. (3.1) into Eq. (3.2). It is $F_\lambda(0,s)\equiv P_\lambda(s)$, $F_\lambda(r,0)\equiv 0$, $F_\lambda(r\geq 1,s=1)=0$, and for $s\geq 1$, $r\geq 1$,

$$\begin{aligned}F_\lambda(r,s+1)=&\lambda(1-\lambda)[F_\lambda(r-1,s)+F_\lambda(r+1,s)]\\&+\lambda^2\sum_{s'=0}^{s}P_\lambda(s-s')[F_\lambda(r-1,s')\\&+F_\lambda(r+1,s')]\\&-\lambda^2\sum_{s'=0}^{s}F_\lambda(r-1,s')F_\lambda(r+1,s-s').\end{aligned}\tag{3.7}$$

Now we will focus on the spatiotemporal correlations at the critical point $\lambda=\lambda_c=1/2$. For sufficiently large values of r and s we will show that $F_\lambda(r,s)\to 0$ for $r\to\infty$ sufficiently fast such that we can neglect the nonlinear term in Eq. (3.7). We can take the continuum limit and obtain [24]

$$\frac{\partial F(r,s)}{\partial s}\sim\frac{1}{2}\nabla_r^2F(r,s)+\frac{1}{2}\int_0^s V(s-s')F(r,s')ds',\tag{3.8}$$

a ''Schrödinger'' equation in imaginary time, for $F(r,s)$ with a nonlocal memory kernel $V(s)=P(s)-2\delta(s)$, where $P(s)=P_{\lambda_c}(s)$ given in Eq. (2.2), and $\delta(s)$ is the usual Dirac δ function. Note that it is the statistical independence of the avalanches for $M\to\infty$ that gives $V(s)$ in terms of the probability distribution of avalanche sizes. The memory in the system here is characterized solely in terms of this distribution.

This nonlocal potential with the integral kernel $V(s)$ contains all of the history dependence of the process. In its absence the system would have no memory and be purely diffusive with a Gaussian tail $F\sim e^{-r^2/2s}$. In its presence the probability to have reached a site at distance r at time s gets contributions from avalanches that reached r at earlier times $s'<s$. These contributions are weighted according to $P(s-s')$ which has a power law tail. Avalanches contributing to $F(r,s)$ consist of subavalanches, one of which reaches r in time s' while the other's combined duration is $s-s'$. The subavalanche tree structure gives a hierarchy of time scales. This changes the relaxation dynamics to be non-Gaussian, and we find as our main result that

$$F_{\lambda_c}(r,s)\sim(24/\pi)^{1/2}s^{-3/2}\left(\frac{r^4}{s}\right)^{1/3}e^{-3/4\,(r^4/s)^{1/3}}\quad(r^4\gg s\gg 1).\tag{3.9}$$

It is immediately clear from the form of the solution that the avalanche dimension for the subdiffusive spreading of activity ($r^D\sim s$) is $D=4$. Diffusion is slowed down because the activity has a tendency to revisit sites, and the system remembers these previously visited sites. Considering $x=r^D/s$ as the scaling variable, the variation of the exponent is much slower with a ''fat'' tail ($\sim x^{1/3}$) compared to a Gaussian tail ($\sim x$ with $D=2$).

In Appendix C we derive the complete leading asymptotic behavior given in Eq. (3.9). Here we will just show how the history dependence in the Schrödinger equation (3.8) gives rise to the non-Gaussian tail in the exponential of Eq. (3.9).

A. Calculation of the fat tail

Using a Laplace transform $\widetilde{F}(r,y)=\int_0^\infty ds e^{-ys}F(r,s)$ Eq. (3.8) turns into an ordinary second-order differential equation in r,

$$\nabla_r^2\widetilde{F}(r,y)\sim[2y-\widetilde{V}(y)]\widetilde{F}(r,y),\tag{3.10}$$

where $\widetilde{V}(y)$ is the Laplace transform of $V(s)$. Since $F(r,s)$ is falling for large r, it is

$$\widetilde{F}(r,y)\sim C(y)\exp[-r\sqrt{2y-\widetilde{V}(y)}],\tag{3.11}$$

and we assume that $C(y)$ is a sufficiently well-behaved function near $y=0$.

The inverse Laplace transform yields a contour integral with a contour extending just to the right ($\eta>0$) of the imaginary y axis

$$F(r,s)\sim\int_{-i\infty+\eta}^{i\infty+\eta}\frac{dy}{2\pi i}C(y)\exp[ys-r\sqrt{2y-\widetilde{V}(y)}].\tag{3.12}$$

The limit of large s corresponds to small values of y where $\widetilde{V}(y)\sim-2\sqrt{y}$ such that $\sqrt{2y-\widetilde{V}(y)}\sim\sqrt{2}y^{1/4}$. Note that the contribution from the left-hand side of Eq. (3.8) does not effect the leading order which merely consists of a balance between the terms on the right-hand side. After rescaling $y\to y/s$ it is

$$F(r,s)\sim\frac{C(0)}{2\pi is}\int_{\mathcal{C}}dy\exp\left[y-\sqrt{2}\left(\frac{r}{s^{1/4}}\right)y^{1/4}\right],\tag{3.13}$$

where $\mathcal{C}$ is a small piece of contour that crosses the real y axis from below just to the right of $y=0$. It emerges that $F(r,s)$ is exponentially cut off when $r\gg s^{1/4}\gg 1$, determining that the avalanche dimension is $D=4$. In that limit, we can perform a steepest-descent analysis of the integral [25]. First, we note that the expression in the exponent has a moving saddle point at $y_0=\frac{1}{4}r^{4/3}s^{-1/3}$. To fix the saddle point, we substitute $y=y_0v$ to obtain

$$F(r,s)\sim\frac{C(0)y_0}{2\pi is}\int_{\mathcal{C}}dv\exp[y_0(v-4v^{1/4})],\tag{3.14}$$

where the contour $\mathcal{C}$ is deformed such that it crosses the real axis on the saddle point at $v_0=1$. To find the steepest-descent path for the contour in the neighborhood of the

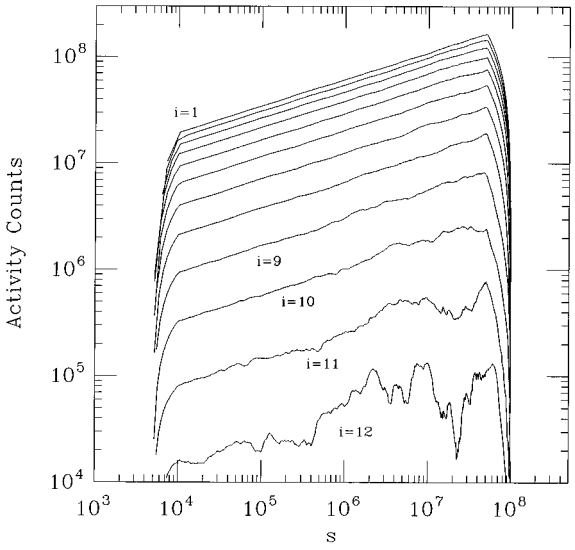

FIG. 6. Counting rates for the activity plotted as a function of time s. Each curve is labeled in descending order by $i=\lceil \log_2 x \rceil$ where $x=r^4/s$ is the scaling variable [see Eq. (3.17)]. Data with $i>12$ has been disregarded due to insufficient statistical accuracy.

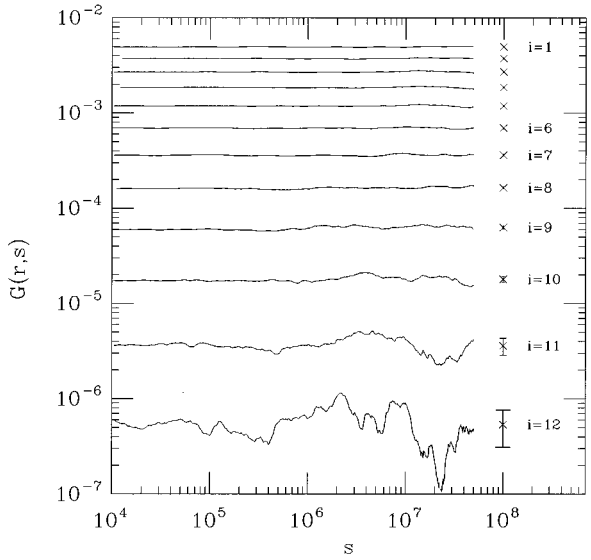

FIG. 7. The normalized distribution of activity $G(r,s)$ derived from Fig. 6. All data ''collapses'' onto plateaus with a mean value for each plateau given by $\times$ on the right, again labeled by $i=\lceil \log_2 x \rceil$. The standard deviation for the data in each plateau is indicated by error bars.

saddle point, we set $v\sim 1+\epsilon+i\delta$ with $\epsilon,\delta\ll 1$. Thus in the exponent, it is $v-4v^{1/4}\sim(-3+\frac{3}{8}\epsilon^2-\frac{3}{8}\delta^2)-i(\frac{3}{4}\epsilon\delta)$, indicating that the steepest-descent path (which is always also a constant-phase path) is given by $\epsilon\equiv 0$ in the neighborhood of the saddle point. Thus, we substitute $v=1+i\delta$ in that neighborhood and obtain the non-Gaussian tail in Eq. (3.9),

$$F(r,s)\sim C'(r,s)\exp\left[-\frac{3}{4}\left(\frac{r^4}{s}\right)^{1/3}\right] \quad (r^4\gg s\gg 1), \tag{3.15}$$

where $C'(r,s)$ only contains powers of r and s. The function $C'(r,s)$, as well as the behavior of $F(r,s)$ for $s\gg r^4\gg 1$, is determined in Appendix C. In Appendix D we will also consider the distribution for avalanches that are fully confined in a box of size r (see Fig. 5) and show that the dominant relaxation behavior is given by Eq. (3.15) as well.

B. Numerical comparison with the propagator

We are now in a position to attempt to compare these results with numerical measurements of the actual propagator $G(r,s)$. Based on earlier numerical investigations [26], we assume that $G(r,s)$ has the scaling form

$$G(r,s)\sim r^{\delta-1}g\left(\frac{r^4}{s}\right) \quad (r^4/s\gg 1). \tag{3.16}$$

At each update s we determine the location r of the minimal random number in a surviving avalanche that started at $s=0,r=0$. We bin counts as a function of ln$s$ and $i=\log_2(r^4/s)$ for avalanches of duration $s<10^8$ (see Fig. 6). We find that the counting rates in logarithmic bins rise linearly with r for each value of i; thus $\delta=1$. In Fig. 7 we plot the normalized data for $G(r,s)$ vs s for different values of i for $10^4<s<5\times 10^7$. Note that all data ''collapses'' onto plateaus whose mean value and standard deviation is given by the crosses with error bars to the right of each curve.

We attempted to numerically determine the asymptotic tail of the function g for large values of $x=r^4/s$ by assuming in accordance with Eq. (3.9) that

$$g(x)\sim e^{-Ax^{\alpha}}, \quad x\gg 1. \tag{3.17}$$

From the sequence of plateau values in Fig. 7 for $g(x)$ we determine a sequence of extrapolants

$$\frac{\ln[-\ln g(x)]}{\ln x}\sim \alpha+\frac{\ln A}{\ln x}, \quad x\gg 1. \tag{3.18}$$

In Fig. 8 we plot this sequence of extrapolants as a function of $1/\ln x$ and estimate that $\alpha=0.35\pm 0.03$, in reasonable agreement with with the value $\alpha=1/3$ from the exponential falloff for $F(r,s)$. Thus the behavior of $G(r,s)$ is consistent with the non-Gaussian asymptotic behavior of the envelope function $F(r,s)$.

IV. SCALING RELATIONS

In the SOC state, spatial and temporal correlations are interrelated. This interrelation is expressed via scaling relations. In a broad class of SOC models, including the evolution models, the knowledge of just two scaling coefficients, such as τ and D, is sufficient to determine any other known coefficient of the SOC state, including the approach to the attractor, through these scaling relations [2]. We have shown in Sec. III that the activity in the SOC state spreads in a subdiffusive manner $r\sim s^{1/D}$, where $D=4$ is the avalanche dimension. In Ref. [17] we have numerically determined the root-mean-square distance of the location of the activity at time s and shown that it scales as $s^{1/4}$. In Fig. 9 we show that the number of sites covered by the activity also grows as

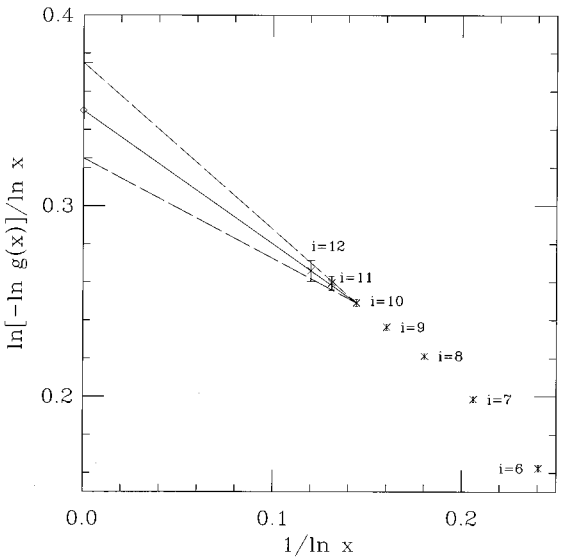

FIG. 8. Plot of the extrapolants from Eq. (3.18) for each $i=\lceil \log_2 x \rceil$ as function of $1/\ln x$. Asymptotically for $1/\ln x \to 0$, this sequence approaches the value of α. From the extrapolation of the sequence to $x \to \infty$ (indicated by the lines that extend the sequence and its errors to the ordinate) we estimate $\alpha = 0.35 \pm 0.03$, in good agreement with $\alpha = 1/3$.

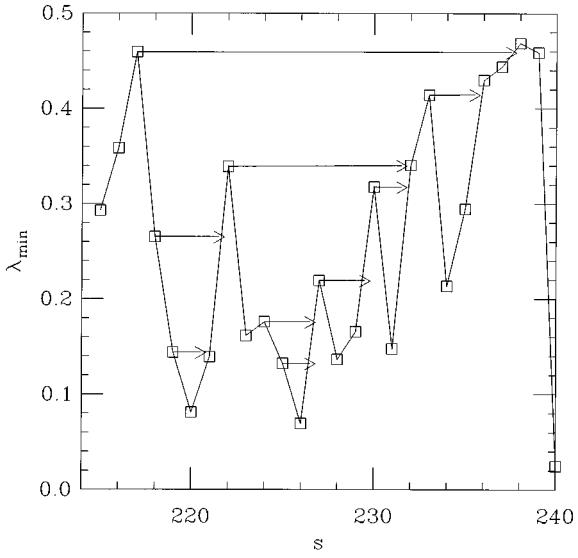

FIG. 10. Plot of a part of the sequence of minimal random numbers $\lambda_{min}(s)$ chosen for an update at time s in a λ_c avalanche for $M=\infty$. The durations of a hierarchy of λ avalanches is indicated by forward arrows, where $\lambda = \lambda_{min}(s)$. Longer avalanches with larger values of λ contain many shorter avalanches which have to finish before the longer avalanche can terminate. Note that an update punctuates any λ avalanche with $\lambda \leqslant \lambda_{min}(s)$.

$s^{1/4}$. This verifies that rather than being multifractal there is only one dimension for the avalanche.

The probability distribution of λ_c avalanche duration is a power law with exponent $\tau = 3/2$, and we have shown that the probability distribution of spatial extents of avalanches is also a power law with critical exponent $\tau_R = 3$. This verifies the scaling relation $\tau_R - 1 = D(\tau - 1)$. It is easy to show that the average size of an avalanche diverges with exponent $\langle s \rangle \sim (\Delta\lambda)^{-\gamma}$ with $\gamma = 1$, and previously we derived that the critical exponent σ describing the cutoff of avalanche sizes below the critical point is 1/2. These results verify the scaling relation $\gamma = (2-\tau)/\sigma$. The result in Sec. III for the cutoff in the correlation length $\nu = 1/2$ in Eq. (3.6) verifies the scaling relation $\nu = 1/(\sigma D)$. Our analysis of the model in higher than one dimension shows that all of these above mentioned exponents are independent of dimension.

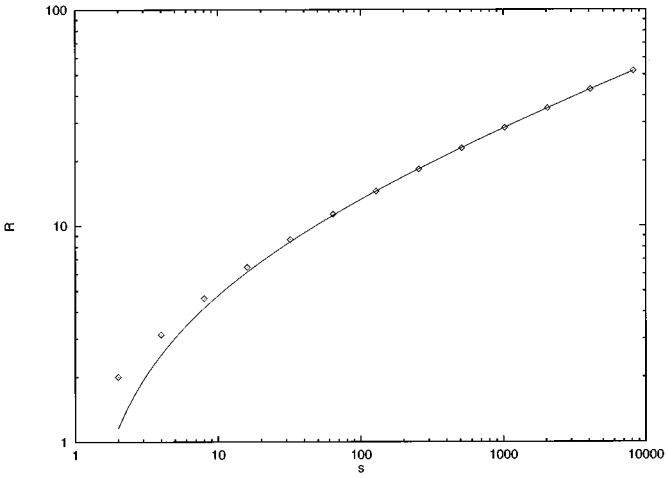

FIG. 9. Plot of the mean width $R(s)$ of the compact region of covered sites for surviving avalanches at time s for $s < 10^5$. The result of a simulation involving 10^8 avalanches is given by $\diamond$, and the solid line is given by $6.10(s^{1/4} - 1.0)$, obtained from an asymptotic fit of the data for large s.

The punctuated equilibrium behavior, however, does depend on dimension. Each site is visited many times in a long lived avalanche. The intervals between subsequent returns to a given site correspond to periods of stasis for a given species. As shown in Fig. 1, the accumulated number of returns to a given site forms a ''Devil's staircase''; the plateaus in the staircase are the periods of stasis for that species. The punctuations, i.e., the times when the number of returns increases, occupy a vanishingly small fraction of the time scale on which the evolutionary activity proceeds. The distribution of plateau sizes is the same as the distribution of first returns of the activity to a given site $P_{\rm FIRST}(s)$. We found in dimensions $d \leqslant 4$ that $P_{\rm FIRST}(s) \sim s^{-\tau_{\rm FIRST}}$ for large s with $\tau_{\rm FIRST} = 2 - d/D$ [2]. For $M \to \infty$ in $d = 1$ dimension, the scaling relations therefore predict $\tau_{\rm FIRST} = 7/4$. We have measured $\tau_{\rm FIRST} = 1.73 \pm 0.05$.

Forward avalanches

The quantity $P_\lambda(s)$ is the conditional probability to have a forward avalanche of size s given that the signal at the starting point was equal to λ. Such avalanches are defined by looking at the first moment forward in time when the signal λ_{min} exceeds its current value λ. It is important to note that this conditional forward probability distribution is exactly equal to the ''punctuating'' avalanche distribution. Punctuating λ avalanches are defined as the intervals separating subsequent instances when $\lambda_{min}(s) \geqslant \lambda$; see Fig. 10. For example, the punctuating $\lambda = 0$ avalanches form a sequence

where all avalanches have size $s=1$. The probability distribution for the λ avalanches does not depend on the precise value of the site that started the λ avalanche (as long as it is $\geqslant\lambda$) because this value is erased from the system after the first update. Thus the minimal numbers selected at different time steps are distributed as

$$p(\lambda_{min}\geqslant\lambda)=1/\langle s\rangle_\lambda \quad \text{where } \langle s\rangle_\lambda=\sum_{s=0}^{\infty} sP_\lambda(s). \tag{4.1}$$

Substituting Eq. (2.2) gives $\langle s\rangle_\lambda=1/(1-2\lambda)$, and $p(\lambda_{min}=\lambda)=2$ for $0\leqslant\lambda\leqslant 1/2$.

The distribution of *all* forward avalanches $P_f^{all}(s)$ is obtained by integrating the conditional probability from Eq. (2.2) with the proper weight $p(\lambda_{min}=\lambda)$ for the starting value of the avalanche [27,28,2]. This distribution measures avalanches *which begin at every time step* s' and end at the first moment forward in time $s'+s$ when $\lambda_{min}(s'+s)>\lambda_{min}(s')$. We find in agreement with numerical simulations that

$$P_f^{all}(s)=\int_0^{1/2} p(\lambda_{min}=\lambda)P_\lambda(s)d\lambda=\frac{A(s)}{s}+\frac{1}{s(2s+1)} \tag{4.2}$$

with $A(s)$ given in Eq. (2.2). For large s this distribution is a power law

$$P_f^{all}(s)\sim s^{-\tau_f^{all}} \quad \text{where } \tau_f^{all}=2. \tag{4.3}$$

This particular exponent τ_f^{all} turns out to be superuniversal and equals 2 for a wide variety of extremal models [28,2].

V. BACKWARD AVALANCHES AND ULTRAMETRICITY

Due to the irreversible nature of the process, it is interesting to consider the properties of the system under time reversal which can be studied in terms of backward avalanches. Now we look for the first moment *back* in time when $\lambda_{min}(s'-s)>\lambda_{min}(s')=\lambda$ [27,28,2]. The definitions of forward and backward avalanches are illustrated in Figs. 10 and 11. These figures demonstrate the hierarchy in the avalanche structure: all forward and backward avalanches that start inside one big forward (backward) avalanche are constrained to not go beyond the limits of the parental avalanche and, therefore, can be considered to be its subavalanches. Each subavalanche in turn has its own subavalanches, and so on. One can look at the entire activity as one great parental critical avalanche, which began in the distant past. It contains subavalanches of all sizes.

We can determine the distributions for λ backward avalanches $P_\lambda^b(s)$ and all backward avalanches $P_b^{all}(s)$ exactly. Suppose we have a temporal sequence $\lambda_{min}(s')$ which is an ensemble of N, λ punctuating avalanches, where N is a sufficiently large number. The average number of λ punctuating avalanches of size s in such an ensemble is given by $N(s)=NP_\lambda(s)$. At the end of any λ avalanche of size s, precisely $(s+1)$ new random numbers have been introduced into the system that were not there when the avalanche began. All these random numbers are *uncorrelated* and uniformly distributed between λ and 1 [2].

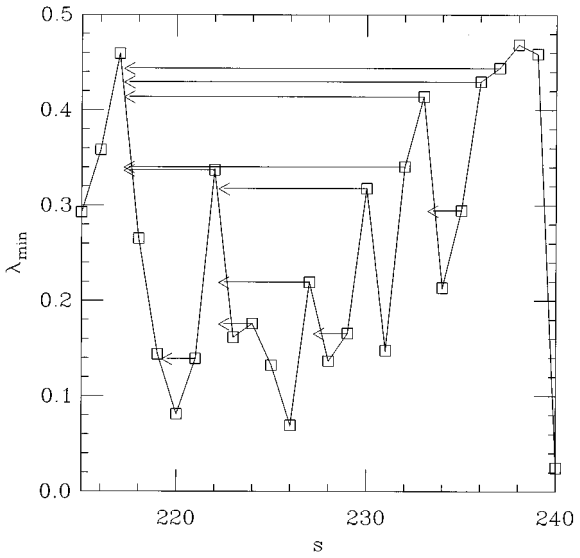

FIG. 11. Same sequence $\lambda_{min}(s)$ as in Fig. 10, where the durations of backward λ avalanches is indicated by backward arrows. A similar hierarchical structure of subavalanches emerges, although with a different distribution than for forward λ avalanches in reflection of the irreversibility of the update process.

To have $\lambda_{min}(s'+s)=\lambda$ we need the minimal number in the system to lie between λ and $\lambda+d\lambda$. This number can be only in this set of new random numbers, since at the beginning of the λ avalanche every number in the system was by definition larger than or equal to λ. The probability that at least one of these new numbers will be between λ and $\lambda+d\lambda$ is given by $(s+1)d\lambda/(1-\lambda)$. Increasing the parameter to $\lambda+d\lambda$, the number N of avalanches will be changed by $dN=-N(s+1)d\lambda/(1-\lambda)$. Of course the sum of the temporal durations of these avalanches will remain constant. This leads to the following differential equation for the average size of an avalanche

$$\frac{d\ln\langle s\rangle_\lambda}{d\lambda}=\frac{(s+1)}{1-\lambda}, \tag{5.1}$$

which is analogous to Eq. (16) in Ref. [2], and also shows that the avalanche size diverges with exponent $\gamma=1$.

The number $N_\lambda^b(s)$ of valid λ backward avalanches of size s in our ensemble of punctuating avalanches is $N_\lambda^b(s)d\lambda=NP_\lambda(s)(s+1)d\lambda/(1-\lambda)$. Therefore, the conditional probability distribution of λ backward avalanches obeys

$$P_\lambda^b(s)=\frac{c(s+1)P_\lambda(s)}{(1-\lambda)}=\frac{c}{\lambda(1-2\lambda)}\frac{d[\lambda^2P_\lambda(s)]}{d\lambda}. \tag{5.2}$$

The proportionality constant c is determined from the normalization condition $\Sigma_{s=0}^{\infty}P_\lambda^b(s)=1$, so that $c=(1-2\lambda)/2$.

The distribution of all backward avalanches measures avalanches which begin at every time step s', and end at the first moment backward in time $s'-s$, when $\lambda_{min}(s'-s)>\lambda_{min}(s')$. We find

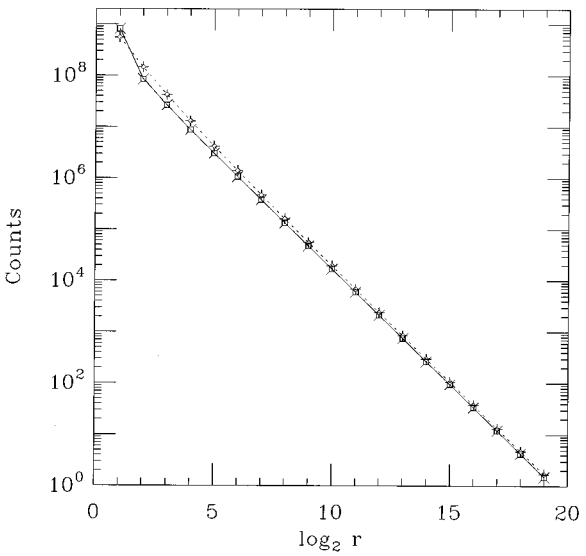

FIG. 12. Log-log plot of the distribution for the duration of backward avalanches (+) and the distribution for the ultrametric distances between subsequent minimal sites (×). Both functions seem to coincide asymptotically for large s.

$$P_b^{all}(s)=\int_0^{1/2} p(\lambda_{min}=\lambda)P_\lambda^b(s)d\lambda$$

$$=\frac{\Gamma(s+1/2)}{2s\Gamma(1/2)\Gamma(s+1)}+\frac{1}{2s(2s+1)}. \qquad (5.3)$$

At large times this distribution is a power law $P_b^{all}(s) \sim s^{-\tau_b^{all}}$ where $\tau_b^{all}=3/2$. Here we have explicitly demonstrated that time reversal symmetry is broken. The forward and backward avalanches have different probability distributions and different scaling limits at large times. Equation (5.3) is in perfect agreement with numerical simulations.

Unless the backward avalanche has size $s=1$, two extremal values that are chosen at subsequent times must have both been present when the first of them was chosen. These two barrier values will have some ultrametric distance between them. This ultrametric distance must be less than or equal to the backward avalanche size, because the extremal value that terminates a backward avalanche must be an ancestor to *all* of the extremal values in that backward avalanche. The probability to have an ultrametric distance larger than s is bounded above by $P_b^{all}(s)$. We have numerically measured the ultrametric distance between subsequent activity and find a power law. In fact, as shown in Fig. 12 it has the same leading asymptotic behavior as P_b^{all} within numerical accuracy.

We conclude by speculating about connections with other phenomena related to glassy dynamics (see also Ref. [21]). The directed polymer in a random media (DPRM) [29], which could be a paradigm for glassy systems, exhibits an ultrametric structure in the optimal paths as well as a non-Gaussian tail for the probability distribution of these paths. These paths are somewhat analogous to the activity pattern in our model. However, unlike the DPRM, our model is inherently dynamical. Tang and Bak [30] found stretched exponential relaxation for the current in a sandpile model of SOC which could indicate that glassy dynamics takes place near a critical point. Recently Stein and Newman [31] have put forward a picture of dynamics on a high dimensional rugged fitness landscape based on an invasion percolation (SOC) picture.

Finally, we note that our model may fit into the picture of hierarchically constrained dynamics put forward by Palmer, Stein, Abrahams, and Anderson [32]. We have an equation of motion for the dynamics which takes place in terms of avalanches spanning all time scales. These avalanches are our hierarchically constrained degrees of freedom. Looking at Fig. 10 one notices that every λ avalanche is composed of subavalanches which are fully contained within it. Each λ avalanche cannot terminate until its subavalanches finish, so that the faster degrees of freedom successively constrain slower ones and form a hierarchy.

ACKNOWLEDGMENTS

This work was supported by the U.S. Department of Energy under Contract Nos. DE-AC02-76-CH00016 and DE-FE02-95ER40923. M.P. thanks the U.S. Department of Energy Distinguished Postdoctoral Fellowship Program for financial support.

APPENDIX A: SOLUTION OF EQ. (3.3)

It is straightforward to solve Eq. (3.3) using a generating function. Defining $p_\lambda(x)=\Sigma_{s=0}^{\infty}x^s P_\lambda(s)$ and applying the initial conditions [see Eq. (3.2)] $P_\lambda(0)=0$ and $P_\lambda(1)=(1-\lambda)^2$, we find

$$p_\lambda(x)-(1-\lambda)^2=2\lambda(1-\lambda)xp_\lambda(x)+\lambda^2 x p_\lambda(x)^2, \qquad (A1)$$

an ordinary quadratic equation for the generating function. Its only acceptable solution is

$$p_\lambda(x)=\frac{[1-\sqrt{1-4\lambda(1-\lambda)x}]^2}{4\lambda^2 x}. \qquad (A2)$$

The solution for $P_\lambda(s)$ in Eq. (2.2) is simply given by the coefficients in x of the Taylor series of $p_\lambda(x)$.

The generating function $p_\lambda(x)$ has a square-root singularity which determines the asymptotic behavior of its Taylor coefficients, i.e., $P_\lambda(s)$. We point out that this asymptotic behavior is a robust feature with respect to changes in the way the model is updated at each time step. For instance, if we had not chosen to set the barrier with the current minimum to unity but to replace it also with a new random number, we would have obtained a cubic equation for $p_\lambda(x)$; the solution of which would still be dominated by a square-root singularity. Furthermore, an update including more than nearest-neighbor sites would lead to even higher-order algebraic equations for $p_\lambda(x)$, which are still dominated by the same square-root singularity. It would be interesting to consider changes in the updating rules that in fact would replace the leading square-root singularity, and the physics that such new rules indicate.

APPENDIX B: CALCULATION OF EQ. (2.4)

Let r be a non-negative integer. Let $N(i,r)$ be the probability that a λ_c avalanche which starts at site i will always be completely contained inside a box of radius r centered at the origin $i=0$. By definition, $N(i,0)\equiv 0$ because in the initial state the avalanche already contains one barrier which certainly will never be contained inside a box of vanishing radius.

The properties of an avalanche starting at i can be related to the properties of avalanches starting at $i-1$ and $i+1$ by considering all possible states of the avalanche after the first step. No new active barriers are created after the first step with probability $(1-\lambda_c)^2=1/4$ and the avalanche terminates without ever spreading beyond the site i. A single new active barrier is created after one time step either to the left or the right of i, each with a probability of $\lambda_c(1-\lambda_c)=1/4$, and $N(i,r)$ is related to $N(i-1,r)$ or $N(i+1,r)$, respectively. Finally, with a probability of $\lambda_c^2=1/4$ two new active barriers are created at $i-1$ and at $i+1$, and the avalanche starting at i will never leave the box if neither avalanche ensuing from $i-1$ and $i+1$ will ever leave the box. Thus, assuming throughout that $r>1$, it is for $|i|<r-1$

$$N(i,r)=\tfrac{1}{4}+\tfrac{1}{4}[N(i-1,r)+N(i+1,r)] + \tfrac{1}{4}N(i-1,r)N(i+1,r). \tag{B1}$$

Clearly, $N(i,r)\equiv 0$ for all $|i|\geqslant r$, leading to the boundary condition for $i=r-1$,

$$N(r-1,r)=\tfrac{1}{4}+\tfrac{1}{4}N(r-2,r). \tag{B2}$$

Since $N(i,r)$ is symmetric in its first argument, we will only consider non-negative values of i and obtain another boundary condition at $i=0$ from Eq. (B1)

$$N(0,r)=\tfrac{1}{4}+\tfrac{1}{2}N(1,r)+\tfrac{1}{4}N(1,r)^2. \tag{B3}$$

We can simplify Eq. (B1) by substituting

$$N(i,r)=1-f(i,r) \tag{B4}$$

to obtain for $0<i<r-1$

$$\Delta_i^2 f(i,r)=\tfrac{1}{2}f(i-1,r)f(i+1,r), \tag{B5}$$

where Δ_i is a difference operator. Equation (B3) leads to a boundary condition at $i=0$,

$$\Delta_i f(i=1,r)=\tfrac{1}{4}f(1,r)^2, \tag{B6}$$

while Eq. (B2) gives another boundary condition for $i=r-1$,

$$\Delta_i f(i=r-1,r)=-\tfrac{3}{4}f(r-2,r)+\tfrac{1}{2}. \tag{B7}$$

To make further progress we assume $r\gg 1$, which allows to consider the continuum limit of Eq. (B5). We set $z=i/r$ such that z is a continuous variable in the unit interval for any r in this limit. We also set $y(z)=f(i,r)$, where y is a function of z that depends on r as a parameter. Thus we can rewrite Eq. (B5) as

$$\frac{1}{r^2}y''(z)=\frac{1}{2}y(z)^2 \tag{B8}$$

to leading order in the limit $r\to\infty$. For the boundary conditions at $z=0$ and $z=1$ we find from Eqs. (B6), (B7)

$$\frac{1}{r}y'(0)=\frac{1}{4}y(0)^2,\quad \frac{1}{r}y'(1)=-\frac{3}{4}y(1)+\frac{1}{2}. \tag{B9}$$

We note that we can obtain an equation for any value of λ

$$\frac{1}{r^2}y''(z)=\left(\frac{1}{\lambda}-2\right)y(z)+\lambda y(z)^2 \tag{B10}$$

which reduces to Eq. (B8) for $\lambda=\lambda_c$. It is easy to show that the linear term dominates on the right-hand side for $\lambda<\lambda_c$, leading to avalanche distributions with an exponential cutoff for large r.

We can integrate Eq. (B8) using standard techniques for autonomous ordinary differential equations [25]. We set $u(y)=y_r'(z)$, use the chain rule to get $y_r''(z)=u'(y)u(y)$, and integrate once to find

$$\frac{1}{r}y'(z)=\pm\sqrt{(1/3)y(z)^3+C}. \tag{B11}$$

Since $y(z)$ is a rising function of z, we choose the positive root. The integration constant C can be rewritten using the boundary condition at $z=0$ in Eq. (B9) as $C=-\frac{1}{3}y(0)^3$, where we neglected terms of higher order in $y(0)$ because $y(0)$ is expected to be small for $r\to\infty$.

Integrating one more time we obtain

$$\int_1^{y(z)/y(0)}\frac{d\zeta}{\sqrt{\zeta^3-1}}=zr\left[\frac{y(0)}{3}\right]^{1/2}. \tag{B12}$$

We find at $z=1$, using Eq. (B9), that $y(1)=2/3$, because $y'(1)/r\ll 1$. Thus $y(1)/y(0)\to\infty$, and we obtain Eq. (2.4)

$$f(0,r)\sim y(0)\sim\frac{3}{r^2}\left(\int_1^\infty\frac{d\zeta}{\sqrt{\zeta^3-1}}\right)^2=\frac{1}{3}\left[\frac{\Gamma(\frac{1}{6})\Gamma(\frac{1}{2})}{\Gamma(\frac{2}{3})}\right]^2\frac{1}{r^2} \approx\frac{17.69}{r^2}. \tag{B13}$$

Note that this result verifies our assumption that $y(0)$ is small. Using dominate balance techniques [25] we can show that this solution is in fact the only consistent solution.

APPENDIX C: LEADING ASYMPTOTIC BEHAVIOR OF THE SPATIOTEMPORAL CORRELATIONS WITH RESPECT TO A PARTICULAR SITE

The nonlinear integro-difference Eq. (3.7) can be solved exactly in the continuum limit. Taking the continuum limit is justified because we are ultimately interested in the behavior of $F(r,s)$ for sufficiently large values of r and s. In general,

to obtain the asymptotic behavior of a difference equation from the corresponding differential equation can be tricky even in the linear case [25]. But comparison with our calculation in Appendix D, where the continuum limit poses no problem, independently confirms our approach here.

With $f(r,x)=\Sigma_{s=0}^{\infty}x^s F_\lambda(r,s)$ and $p(x)=\Sigma_{s=0}^{\infty}x^s P_\lambda(s)$ as generating functions, we obtain from Eq. (3.7), using Eq. (A2),

$$\Delta_r^2 f(r,x)=A(x)f(r,x)+B(x)f(r-1,x)f(r+1,x),$$

$$f(0,x)=p(x), \quad \text{and} \quad f(\infty,x)=0, \tag{C1}$$

defining

$$A(x)=\frac{1-2x\lambda(1-\lambda)-2x\lambda^2 p(x)}{x\lambda(1-\lambda)+x\lambda^2 p(x)},$$

$$B(x)=\frac{x\lambda^2}{x\lambda(1-\lambda)+x\lambda^2 p(x)}. \tag{C2}$$

We can take the continuum limit of Eq. (C1) and get to leading order for large r an ordinary second-order nonlinear differential equation for f as a function of r

$$f(r)''=Af(r)+Bf(r)^2, \quad f(0)=p, \quad f(\infty)=0, \tag{C3}$$

where we have suppressed dependence on the parameter x. Using again the techniques for autonomous equations (see Appendix B) and the fact that $f(\infty)=0$, Eq. (C3) can be solved exactly to give

$$f(r)=p\left[\cosh\left(\frac{1}{2}\sqrt{A}r\right)+\left(1+\frac{2Bp}{3A}\right)^{1/2}\sinh\left(\frac{1}{2}\sqrt{A}r\right)\right]^{-2}. \tag{C4}$$

Thus we obtain from Eq. (C4) a closed-form expression for the envelope function of the spatiotemporal distribution of avalanches

$$F_\lambda(r,s)\sim-\oint\frac{dx}{2\pi i}x^{-s-1}f(r,x), \tag{C5}$$

where the contour encircles a small neighborhood of the origin in the complex x plane in the positive direction.

From now on, we only consider the critical case $\lambda=\lambda_c=1/2$. The integrand in Eq. (C5) can be expanded for large s in the neighborhood of $x=1$ by substituting $x=1-u/s$. Then the integration for u follows a contour that crosses the positive real axis from above near the origin in the complex-u plane. With

$$p(x)\sim 1-2\left(\frac{u}{s}\right)^{1/2}+2\frac{u}{s},$$

$$A\sim 2\left(\frac{u}{s}\right)^{1/2}+2\frac{u}{s},$$

$$B=\frac{1}{2}+\frac{1}{2}\left(\frac{u}{s}\right)^{1/2}, \tag{C6}$$

we find

$$F(r,s)\sim\int_{\mathcal{C}}\frac{du}{2\pi i s}e^u f\left(r,1-\frac{u}{s}\right), \tag{C7}$$

where an analysis of Eq. (C4) yields

$$f\left(r,1-\frac{u}{s}\right)\sim\begin{cases}\dfrac{12}{r^2}\left[-\left(\dfrac{u}{s}\right)^{1/2}\left(\dfrac{r^2}{6}+1\right)+\left(\dfrac{u}{s}\right)^{3/2}\dfrac{r^6}{756}+\cdots\right] & (1\ll r^4\ll s),\\ 24\left(\dfrac{u}{s}\right)^{1/2}\exp\left[-\sqrt{2}r\left(\dfrac{u}{s}\right)^{1/4}\right] & (s\ll r^4).\end{cases} \tag{C8}$$

In the first case of Eq. (C8) we have neglected terms with integer powers in u which would vanish in the following integration.

For $r^4\gg s$, we evaluate the integral for $F(r,s)$ by steepest-descent analysis similar to Sec. III, but taking account also of the nonexponential factor in the integrand. For $1\ll r^4\ll s$, we use Hankel's contour integral representation of the Γ function [33]

$$\frac{1}{\Gamma(-\nu)}=-\int_{\mathcal{C}}\frac{du}{2\pi i}e^u u^\nu \tag{C9}$$

to find

$$F(r,s)\sim\begin{cases}\dfrac{1}{\sqrt{\pi}}s^{-3/2}\left(1+\dfrac{6}{r^2}+\dfrac{1}{84}\dfrac{r^4}{s}+\cdots\right) & (1\ll r^4\ll s),\\ \sqrt{\dfrac{24}{\pi}}s^{-3/2}\left(\dfrac{r^4}{s}\right)^{1/3}\exp\left[-\dfrac{3}{4}\left(\dfrac{r^4}{s}\right)^{1/3}\right] & (r^4\gg s\gg 1),\end{cases} \tag{C10}$$

where the second case is our main result for the non-Gaussian tail given in Eq. (3.9).

APPENDIX D: LEADING ASYMPTOTIC BEHAVIOR OF THE SPATIOTEMPORAL CORRELATIONS WITH RESPECT TO A BOX

In this appendix we calculate the distribution for the size of a box in space and time such that a λ avalanche will be fully contained in it. This notion, which easily generalizes to higher dimensions, extends on the calculation in Sec. III and Appendix C, where we only considered avalanches with respect to a single site. While the calculation here (which is similar to Appendix B) is somewhat more extensive, the results are virtually identical and justify our simplified approach in Sec. III.

Let $P(r,s,i)$ be the probability for a λ avalanche, which starts at time $s=0$ with a single active barrier on site i, to have no active barriers for the first time at time s, and to not have left a box $i\in(-r,r)$. We merely consider avalanches in the critical state and set $\lambda=\lambda_c=1/2$. By definition, $P(r=0,s,i)\equiv 0$ for all $s\geqslant 0$. Furthermore, $P(r,s=0,i)\equiv 0$ for all r, because by definition no avalanche ends at time $s=0$. Ultimately, we want to find the distribution $F(r,s,0)$ of avalanches of duration s that start at the origin $i=0$ and are completely contained in a box of radius r. A generic avalanche is plotted in Fig. 5; the smallest box it is fully contained in is of size $r=18$ in this case. In correspondence with Eq. (3.1) it is

$$F(r,s,i)=P(r=\infty,s,0)-P(r,s,i), \tag{D1}$$

where $P(r=\infty,s,0)=P_\lambda(s)$ is given in Eq. (2.2).

As before, the properties of an avalanche that originates at $s=0$ can be deduced from the properties of avalanches that ensue after the first update. The original avalanche can either terminate after the first update when the update does not produce any new active barriers with probability $(1-\lambda)^2=1/4$, or it can generate new avalanches by creating new active barriers. If the first update creates exactly one new barrier with likelihood $\lambda(1-\lambda)=1/4$ either to the left or to the right of site i, the properties of an original avalanche of duration s is related to the properties of an avalanche of duration $s-1$ with regard to a site of distance $i-1$ or $i+1$, respectively. If the first update creates two new active barriers with probability $\lambda^2=1/4$ to the left and the right of site i, two new avalanches ensue. Then, the properties of the original avalanche of duration s is related to the properties of all combinations of two avalanches of combined duration $s-1$. For any such combination, the probability to not leave the box when starting at site i is given simply by the product of the probabilities for the two ensuing avalanches to not leave the box after starting at site $i-1$ or $i+1$, respectively. We thus obtain for $r\geqslant 1$ and $|i|<r$ that $P(r,s=1,i)=1/4$, and for all $s\geqslant 1$ that

$$P(r,s+1,i)=\frac{1}{4}[P(r,s,i-1)+P(r,s,i+1)]+\frac{1}{4}\sum_{s'=0}^{s}P(r,s',i-1)P(r,s-s',i+1). \tag{D2}$$

Since $P(r,s,i)$ is symmetric in i, we restrict ourselves to non-negative values of i, leading to a boundary condition at $i=0$:

$$P(r,s+1,0)=\frac{1}{2}P(r,s,1)+\frac{1}{4}\sum_{s'=0}^{s}P(r,s',1)P(r,s-s',1) \quad (s\geqslant 1,r\geqslant 1). \tag{D3}$$

Since $P(r,s,i\geqslant r)\equiv 0$, we obtain a second boundary condition at $i=r-1$:

$$P(r,s-1,r-1)=\frac{1}{4}P(r,s,r-2) \quad (s\geqslant 1,r\geqslant 2). \tag{D4}$$

Using Eq. (D1), and defining $f(r,x,i)=\Sigma_{s=0}^{\infty}x^sF(r,s,i)$, we obtain for $1\leqslant i\leqslant r-2$

$$\Delta_i^2 f(r,x,i)=A(x)f(r,x,i)+B(x)f(r,x,i-1)f(r,x,i+1), \tag{D5}$$

where $A(x)$ and $B(x)$ are the same as in Eq. (C2), supplemented by the boundary conditions

$$\Delta_i f(r,x,i=1)=\left[1-\frac{x}{4}-\frac{x}{4}p(x)\right]f(r,x,1)+\frac{x}{4}f(r,x,1)^2,$$

$$\Delta_i f(r,x,i=r-1)=\left(\frac{x}{4}-1\right)f(r,x,r-2)-p(x)\left(1-\frac{x}{4}\right)-\frac{x}{4}. \tag{D6}$$

As before in Appendix C, we expand the equations in the limit $x\to 1$ to analyze the avalanche distribution for large times s. Then Eq. (D5) simplifies for $1\leqslant i\leqslant r-2$ to

$$\Delta_i^2 f(r,x,i)\sim 2\sqrt{1-x}f(r,x,i)+\tfrac{1}{2}f(r,x,i-1)f(r,x,i+1) \tag{D7}$$

with the boundary conditions

$$\Delta_i f(r,x,i=1)\sim\sqrt{1-x}f(r,x,1)+\tfrac{1}{4}f(r,x,1)^2,$$

$$\Delta_i f(r,x,i=r-1)\sim-\tfrac{3}{4}f(r,x,r-2)+\tfrac{1}{2}. \tag{D8}$$

For sufficiently large r, we can take the continuum limit of these equations where $f(r,x,i)\to y(z)/r^2$ with $z=i/r$ as a continuous variable in the unit interval. Equations (D7) then approach

$$y''(z)=2r^2\sqrt{1-x}y(z)+\tfrac{1}{2}y(z)^2,$$

$$y'(0)=r\sqrt{1-x}y(0),$$

$$y(1)=\tfrac{2}{3}r^2. \tag{D9}$$

We can obtain a first integral of Eq. (D9) using again the technique for autonomous equations:

$$y'(z)=\pm\left\{\frac{1}{3}[y(z)^3-y(0)^3]+2r^2(1-x)^{1/2}\times[y(z)^2-y(0)^2]\right\}^{1/2}, \tag{D10}$$

assuming that $y'(0)\to 0$ for $r\to\infty$ sufficiently fast. Since $y(z)$ is a rising function of z, we have to chose the positive root. Integrating again, and using $y(1)$, we obtain

$$\int_1^{2r^2/3y(0)} \frac{d\zeta}{\sqrt{\zeta^3-1+\alpha(\zeta^2-1)}} \sim \left[\frac{y(0)}{3}\right]^{1/2} z$$

$$\text{with} \quad \alpha = \frac{6r^2\sqrt{1-x}}{y(0)}. \tag{D11}$$

For $y(0)\ll r^2\sqrt{1-x}$, i.e., $\alpha\gg 1$, we get

$$\left[\frac{y(0)}{3}\right]^{1/2} \sim \frac{1}{\sqrt{\alpha}} \ln\left[\frac{3}{2}\alpha\right], \tag{D12}$$

which yields

$$f(r,x,0) \sim \frac{y(0)}{r^2} \sim 3\sqrt{1-x}\exp(-\sqrt{2}r(1-x)^{1/4})$$

$$[1\ll r(1-x)^{1/4}], \tag{D13}$$

and by steepest-descent analysis as before

$$F(r,s,0) \sim C(r,s)\exp\left[-\frac{3}{4}\left(\frac{r^4}{s}\right)^{1/3}\right], \quad (1\ll s\ll r^4) \tag{D14}$$

confirming the non-Gaussian tail found in Eq. (3.9). A similar consideration of the integral in Eq. (D11) would determine the behavior for $r^2\gg y(0)\gg r^2\sqrt{1-x}$, i.e., $\alpha\ll 1$.

[1] P. Bak, C. Tang, and K. Weisenfeld, Phys. Rev. Lett. **59**, 381 (1987); Phys. Rev. A **38**, 364 (1988).

[2] M. Paczuski, S. Maslov, and P. Bak, Phys. Rev. E **53**, 414 (1996); Phys. Rev. Lett. **74**, 4253 (1995); Europhys. Lett. **27**, 97 (1994); **28**, 295 (1994); S. Maslov, M. Paczuski, and P. Bak, Phys. Rev. Lett. **73**, 2162 (1994).

[3] P. Bak and M. Paczuski, Proc. Natl. Acad. Sci. **92**, 6689 (1995).

[4] B. Gutenberg and C. F. Richter, Ann. Geofis. **9**, 1 (1956).

[5] P. Bak and C. Tang, J. Geophys. Res. B **94**, 15 635 (1989); Z. Olami, H. J. S. Feder, and K. Christensen, Phys. Rev. Lett. **68**, 1244 (1992); K. Christensen and Z. Olami, Phys. Rev. A **46**, 1829 (1992); J. Carlson and J. Langer, Phys. Rev. Lett. **62**, 2632 (1989).

[6] *Fractals in the Earth Sciences,* edited by C. C. Barton and P. R. Lapointe (Plenum, New York, 1994).

[7] S. J. Gould and N. Eldredge, Paleobiology **3**, 114 (1977); Nature **366**, 223 (1993).

[8] K. Sneppen, P. Bak, H. Flyvbjerg, and M. H. Jensen, Proc. Natl. Acad. Sci. **92**, 5209 (1995).

[9] P. Bak and K. Sneppen, Phys. Rev. Lett. **71**, 4083 (1993).

[10] P. Bak and M. Paczuski, in Physics of Biological Systems, Lecture Notes in Physics (Springer-Verlag, Heidelberg, in press).

[11] K. Ito, Phys. Rev. E **52**, 3232 (1995).

[12] S. B. Lowen and M. C. Teich, Phys. Rev. E **47**, 992 (1993).

[13] D. Wilkinson and J. F. Willemsen, J. Phys. A **16**, 3365 (1983).

[14] K. Sneppen, Phys. Rev. Lett. **69**, 3539 (1992).

[15] S. I. Zaitsev, Physica A **189**, 411 (1992).

[16] M. E. J. Newman and B. W. Roberts, Proc. R. Soc. London B **260**, 31 (1995); K. Schmoltzi and H. G. Schuster, Phys. Rev. E **52**, 5273 (1995); R. V. Solé and S. C. Manrubia (to be published); N. Vandewalle and M. Ausloos, J. Phys. (France) I **5**, 1011 (1995).

[17] S. Boettcher and M. Paczuski, Phys. Rev. Lett. **76**, 348 (1996).

[18] H. Flyvbjerg, K. Sneppen, and P. Bak, Phys. Rev. Lett. **71**, 4087 (1993); J. de Boer, B. Derrida, H. Flyvbjerg, A. D. Jackson, and T. Wettig, Phys. Rev. Lett. **73**, 906 (1994); J. de Boer, A. D. Jackson, and T. Wettig, Phys. Rev. E **51**, 1059 (1995).

[19] S. A. Kauffman, *Origins of Order: Self-Organization and Selection in Evolution* (Oxford University Press, Oxford, 1992).

[20] R. Rammal, G. Toulouse, and M. A. Virasoro, Rev. Mod. Phys. **58**, 765 (1986).

[21] M. Paczuski and S. Boettcher, COND-MAT/9603085.

[22] C. Darwin, *The Origin of Species by Means of Natural Selection*, 6th ed. (Murray, London, 1910).

[23] S. Boettcher and M. Paczuski (unpublished).

[24] The origin of the factor preceding the Laplacian is not trivial. This term in Eq. (3.8) reads in more detail $\frac{1}{4}\int_0^s ds'\sigma(s-s')\nabla_r^2 F(r,s')$ with $\sigma(s)=P(s)+2\delta(s)$ as a nonlocal diffusion constant. For large s the effect of σ becomes local, leading to the given equation.

[25] C. M. Bender and S. A. Orszag, *Advanced Mathematical Methods for Scientist and Engineers* (McGraw-Hill, New York, 1978).

[26] See Fig. 1 in Ref. [17].

[27] S. Roux and E. Guyon, J. Phys. A **22**, 3693 (1989).

[28] S. Maslov, Phys. Rev. Lett. **74**, 562 (1995).

[29] T. Halpin-Healy and Y.-C. Zhang, Phys. Rep. **254**, 215 (1995).

[30] C. Tang and P. Bak, Phys. Rev. Lett. **60**, 2347 (1988).

[31] See also, D. L. Stein and C. M. Newman, Phys. Rev. E **51**, 5228 (1995).

[32] R. G. Palmer, D. L. Stein, E. Abrahams, and P. W. Anderson, Phys. Rev. Lett. **53**, 958 (1984).

[33] *Handbook of Mathematical Functions,* edited by M. Abramowitz and I. A. Stegun (Dover, New York, 1972), p. 255.